Muon-Induced Single-Event Upsets in 20-nm SRAMs: Comparative Characterization With Neutrons and Alpha Particles

Takashi Kato, Motonobu Tampo, Soshi Takeshita, Hiroki Tanaka, Hideya Matsuyama, Masanori Hashimoto, *Senior Member, IEEE*, and Yasuhiro Miyake

***Abstract*— Negative and positive muon-induced single-event upsets (SEUs) are studied in 20-nm bulk planar SRAMs. Muon irradiation is performed using a mono-energetic source with varying the muon energy. The energy dependence of the cross sections (CSs) of SEUs and multiple-cell upsets (MCUs) shows the significant contribution of muon capture reactions for the negative muon, as reported in previous studies. Interestingly, MCU events are found for the positive muon, in contrast to the previous studies. The CSs for the negative and positive muons are compared with that for the other terrestrial radiations: high-energy neutrons, thermal neutrons, and alpha particles. The voltage dependence of the SEU CS, together with the empirical model for charge collection, demonstrates the difference in the contributing secondary ions among the negative muon, the high-energy neutron, and the thermal neutron. The MCU events are thoroughly analyzed in terms of their ratio to the total events and their fail bit patterns. The results reveal that the MCU characteristics for the negative muon are different from that for the other terrestrial radiations due to the muon capture reactions, where parasitic bipolar effects and the isotropic emission of secondary ions are important factors.**

***Index Terms*— Alpha particle, CMOS, high-energy neutron, multiple-bit upset (MBU), multiple-cell upset (MCU), negative muon, parasitic bipolar effect (PBE), positive muon, single-event upset (SEU), SRAM, thermal neutron.**

I. Introduction

MUONS have received increasing attention as a source of soft errors in the terrestrial environment, where negative and positive muons are produced as secondary cosmic-rays through interactions between primary cosmic rays and the atmosphere. One reason for this increased attention is that scaled semiconductor devices have become sensitive to low-linear energy transfer (LET) particles due to the decreased critical charge. Another reason is that the muons are the most abundant particles among terrestrial cosmic-rays [1]. As a result, there is a growing concern that the negative and positive muons could become a significant source of the terrestrial soft errors [2], [3].

Recent irradiation experiments demonstrated that both the negative and positive muons induce single-event upsets (SEUs) in deep-submicrometer SRAM devices [4]–[7]. One of the important observations in these experiments was that the SEU cross section (CS) is higher for the negative muon than for the positive muon, although the LET is nearly identical between the negative and positive muons. This higher CS for the negative muon was clearly explained by muon capture reactions, which are absent for the positive muon. Through the capture reaction, the negative muon can produce secondary ions with higher LET than the negative muon itself.

In particular, it was shown that the negative muon induces considerable multiple-cell upsets (MCUs) in 65- and 28-nm bulk planar SRAMs, while the positive muon does not [4], [6]. The MCUs are a reliability concern in SRAM devices because multiple-bit upsets (MBUs), which are the MCUs with multiple fail bits in the same logical word, can cause malfunctions even when error correction codes are implemented. The important points here are that the MCU susceptibility increases with the shrinkage of the SRAM cells, and that due to the miniaturization of transistors the MCU mechanism becomes complicated, such as parasitic bipolar effects (PBEs) induced by well-potential perturbation [8], [9]. Therefore, it is required to investigate the muon-induced MCUs in more advanced devices.

In the terrestrial environment, neutrons and alpha particles have been recognized as major sources of the SEUs and MCUs in recent SRAM devices [10]. The neutrons are secondary cosmic-rays and include high-energy and thermal components. Unlike the high-energy neutron, the sensitivity to the thermal neutron depends on the abundance of ^{10}B atoms in device materials [11]. It has been reported that recent manufacturing processes cause the introduction of the ^{10}B atoms, which makes SRAM devices sensitive to the thermal neutron [12]–[14]. The alpha particle is from radioiso-

Manuscript received March 31, 2021; revised May 2, 2021; accepted May 13, 2021. Date of publication May 21, 2021; date of current version July 16, 2021. This work was supported in part by the JST-OPERA Program, Japan, under Grant JPMJOP1721.

Takashi Kato is with the Reliability Engineering Department, Socionext Inc., Kawasaki 213-0012, Japan, and also with the Department of Information Systems Engineering, Osaka University, Osaka 565-0871, Japan (e-mail: kato.takashi@socionext.com).

Motonobu Tampo, Soshi Takeshita, and Yasuhiro Miyake are with the Muon Science Laboratory, High Energy Accelerator Research Organization, Tokai 319-1106, Japan.

Hiroki Tanaka is with the Institute for Integrated Radiation and Nuclear Science, Kyoto University, Osaka 590-0494, Japan.

Hideya Matsuyama is with the Reliability Engineering Department, Socionext Inc., Kawasaki 213-0012, Japan.

Masanori Hashimoto is with the Department of Information Systems Engineering, Osaka University, Osaka 565-0871, Japan.

Color versions of one or more figures in this article are available at https://doi.org/10.1109/TNS.2021.3082559.

Digital Object Identifier 10.1109/TNS.2021.3082559

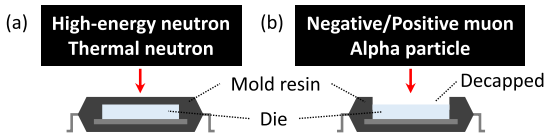

Fig. 1. Irradiation configurations. (a) Neutron irradiation. (b) Muon and alpha particle irradiation.

topic impurities naturally present in device materials, such as packages.

To characterize the muon-induced SEUs and MCUs, it would be beneficial to compare them with those for the other terrestrial radiations: the high-energy neutron, the thermal neutron, and the alpha particle. Previous studies estimated that, in the terrestrial environment, the SEU rates of modern SRAM devices are significantly lower for the muons than for the neutrons [15]–[17]. Nevertheless, since the SEU mechanisms of the neutrons and the alpha particle are well-established, this comparison will provide a better understanding of the mechanism of the muon-induced SEUs. Gasiot *et al.* [16] experimentally characterized SEUs induced by the positive muon, the high-energy neutron, the thermal neutron, and the alpha particle in 28-nm bulk and SOI SRAMs. Liao *et al.* [18] experimentally demonstrated the similarity in SEU and MCU characteristics between the negative muon and the high-energy neutron in 65-nm bulk SRAMs. However, at the present time, there have been no experimental studies comparing SEU and MCU characteristics for the negative and positive muons with that for all the other terrestrial radiations.

In this context, this work investigates the negative and positive muon-induced SEUs and MCUs in 20-nm bulk planar SRAMs, along with a comparison to the high-energy neutron, the thermal neutron, and the alpha particle. The SEU and MCU CSs are statistically evaluated by irradiation tests using mono-energetic muon beams, atmospheric-like neutron beams, and an alpha-ray source. The CSs for the muons are analyzed in terms of their energy and supply voltage dependence, and are then compared with that for the other particles. To explore the MCU characteristics, the MCU events are thoroughly analyzed with respect to the multiplicity and the fail bit pattern. The underlying mechanisms are discussed through the characterization of the muon-induced SEUs and MCUs.

II. Experimental Setup

A. Tested Device and Operation

The test vehicle was SRAM chips fabricated in a 20-nm bulk planar CMOS process. The package type was a standard plastic quad flat package. As illustrated in Fig. 1, the SRAM chips were irradiated from the top. The chips for muon and alpha particle irradiations were decapped [see Fig. 1(b)].

The SRAM operation during the irradiation consisted of write, hold, and read cycles in this order. This operation was a static mode with no write and read functions during the hold cycle. The supply voltage in the hold cycle was varied from 0.35 to 1.0 V to investigate the voltage dependence of the SEU and MCU CSs. The number and physical addresses of fail bits were collected in the read cycle.

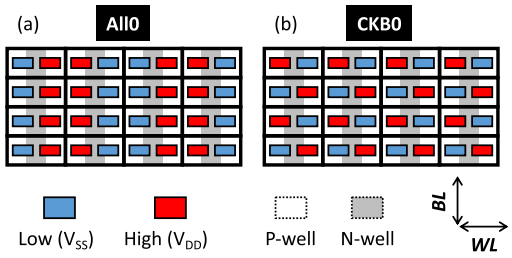

Fig. 2. SRAM node voltages for (a) All0 and (b) CKB0 patterns. Rectangular cells correspond to SRAM cells. Vertical and horizontal directions are parallel to bit lines (BLs) and word lines (WLs), respectively. Blue and red rectangular boxes denote internal nodes of low (V_{SS}) and high (V_{DD}) voltages, respectively. White and gray regions depict p-wells and n-wells, respectively.

TABLE I
Incident Particles and Irradiation Facilities

Incident particle	Energy	Facility
Negative/Positive muon	Monoenergetic	MUSE [19]
High-energy neutron	Atmospheric-like	RCNP [21]
Thermal neutron	Atmospheric-like	KUR [23]
Alpha particle	5.4 MeV	Lab. (^{241}Am)

In this operation, the SRAM chips were written with two types of data patterns, labeled as All0 and CKB0. In the case of the All0 pattern, a logical "0" was written in all the bits. In the case of the CKB0 pattern, logical "0" and "1" were physically arranged in a checkerboard fashion, where "0" was written in the first bit. The arrangements of node voltages for the All0 and CKB0 patterns are explained in Fig. 2(a) and (b), respectively. In each figure, a 4×4 SRAM array is depicted with rectangular cells, where blue and red boxes represent low (V_{SS}) and high (V_{DD}) states of internal nodes, respectively.

B. Irradiation Testing

Irradiation tests were carried out for the negative muon, the positive muon, the high-energy neutron, the thermal neutron, and the alpha particle. The incident particles and the corresponding facilities are summarized in Table I.

1) Negative and Positive Muons: The negative and positive muon irradiations were performed using a monoenergetic muon beam at the D2 beamline of the muon science facility (MUSE) in the Materials and Life Science Experimental Facility of the J-PARC [19]. The energy distribution was Gaussian with a standard deviation of $\sim 5\%$. To minimize muon scattering that occurs before the muons reach the Si die, the irradiations were conducted in helium gas and the mold resin above the Si die was removed [see Fig. 1(b)]. To investigate the energy dependence of the SEU and MCU CSs, the muon energy was varied from 0.84 to 1.46 MeV, which corresponds to the momentum range from 13.4 to 17.7 MeV/c. The muon flux was estimated for each energy by measuring muon decay electrons and positrons, and also by analyzing muonic X-rays using a graphite specimen [20]. The estimated flux at 1.46 MeV, for example, was $\sim 1 \times 10^2/\text{cm}^2/\text{s}$.

2) High-Energy Neutron: The high-energy neutron irradiation was performed using a spallation neutron beam at the WN course of the Research Center for Nuclear Physics (RCNP),

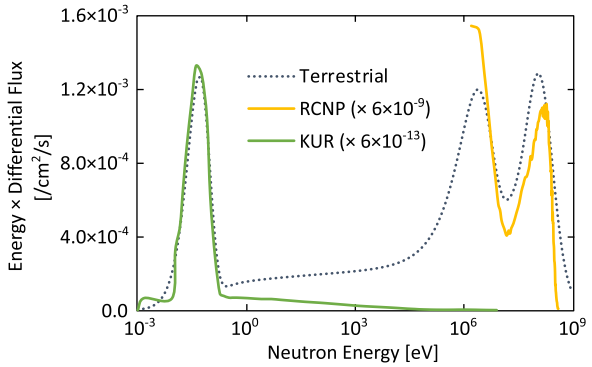

Fig. 3. Energy spectra of the terrestrial neutron [24], the spallation neutron beam at RCNP [21], and the thermal neutron beam at KUR [23].

Osaka University [21]. The energy spectrum of this beam was similar to that of the terrestrial neutron in the energy range from 1 to 300 MeV, as shown in Fig. 3. The integrated neutron flux above 10 MeV was $\sim 7.0 \times 10^6$/cm^2/s. Note that the most of data for the high-energy neutron irradiation was obtained from our previous work [22].

3) Thermal Neutron: The thermal neutron irradiation was performed using a neutron irradiation field at the Heavy Water Neutron Irradiation Facility (HWNIF) of the Kyoto University Research Reactor (KUR) [23]. The energy spectrum of this beam was similar to that of the terrestrial neutron in the thermal energy range, as presented in Fig. 3. The integrated neutron flux below 0.5 eV, which was measured using gold activation wires, was $\sim 2.0 \times 10^8$/cm^2/s. The thermal neutron sensitivity of the test chip was confirmed by performing the irradiations with and without boron shields.

4) Alpha Particle: The alpha particle irradiation was performed using an ^{241}Am source in our laboratory. The nominal energy of the emitted alpha particles was 5.4 MeV. The source was placed above the decapped chip [see Fig. 1(b)]. The particle flux at the surface of the Si die was estimated as $\sim 2.9 \times 10^2$/cm^2/s.

C. CS Calculation

The single-bit upset (SBU) and MCU events were extracted separately according to the spatial distribution of the fail bits. In addition, we analyzed the MBU events which correspond to the MCU events with multiple fail bits in the same WL. It should be noted that the number of the fail bits accumulated during one hold cycle was kept small enough to avoid misinterpreting multiple SBU events as an MCU event.

The SEU, SBU, MCU, and MBU CSs were calculated as $N_{\text{event}}/(\Phi \times N_{\text{bit}})$, where Φ and N_{bit} are the incident particle fluence and the number of SRAM bits irradiated, respectively. N_{event} is the number of observed events for the SEUs, SBUs, MCUs, and MBUs. Here, the SEU events correspond to the sum of the SBU and MCU events.

III. Results and Discussion

A. Muon Energy Dependence of SEU, SBU, and MCU CSs

The muon irradiation with varying the incident energy confirmed the strong energy dependence of the CSs for the negative and positive muons. Fig. 4(a)–(c) present the energy dependence of the SEU, SBU, and MCU CSs, respectively. In this investigation, to maximize the SEU response to the energy change, the supply voltage was set to 0.35 V, which was much lower than the typical operation range. The data pattern was the All0 pattern.

The SEU CS showed a clear peak at 1.02 MeV for both the negative and positive muons, as seen in Fig. 4(a). This CS-peak energy probably corresponds to the case where the position of the Bragg peak of the muon beam is close to the position of the transistors of the SRAM cells. In this case, the charge deposition due to the direct ionization of the muons becomes maximum at the transistors, and hence the SEU events are more likely to occur. Our results clearly demonstrated the coincidence of the CS-peak energy between the negative and positive muons. This reflects the almost identical ranges and LETs of these muons. A similar energy dependence was observed in the previous studies [4], [5].

Although the SBU CS was comparable between the negative and positive muons, the MCU CS for the negative muon was significantly higher than that for the positive muon, as seen in Fig. 4(b) and (c). This difference stems from the muon capture reactions of the negative muon, as discussed in [4]. The capture reactions can produce secondary ions whose LETs are higher than that of the primary muons. This results in a large amount of charge deposition on the transistors. Furthermore, the produced ions are emitted isotropically regardless of the incident direction of the negative muons. In this case, some of these ions travel along the plane of the SRAM array, and hence their tracks can cover the multiple SRAM cells. Therefore, the higher MCU CS for the negative muon than for the positive muon obviously indicates the considerable contribution of the capture reactions for the negative muon.

An interesting observation was that MCU events were found in the positive muon irradiation, as confirmed in Fig. 4(c). In Liao's results previously reported for 65-nm bulk planar SRAMs, no MCU events were observed even at the low voltage condition of 0.4 V [4]. In our results for the 20-nm bulk planar SRAMs, on the other hand, the MCU events were observed at 0.35 and 0.6 V [see also Fig. 5(b)]. This discrepancy can be understood as the scaling effect of the SRAM cells, where the smaller cells are more susceptible to the MCUs induced by charge sharing [25]. Our results thus suggest that the positive muon becomes a possible source of the MCUs in highly-scaled SRAM devices.

In the following investigations, the muon energy was fixed to the CS-peak energy, 1.02 MeV, for both the negative and positive muons. This aims to fully capture the muon-specific characteristics and to consider the worst case situation for the SEU and MCU occurrence. In other words, the following investigations do not focus on the assessment of SEU rates in the terrestrial environment, which requires the consideration of the broad energy spectrum of terrestrial muons [15]–[17].

B. Supply Voltage Dependence of SEU, MCU, and MBU CSs

The comparison of the CSs among the incident particles demonstrated similarities and differences in the voltage

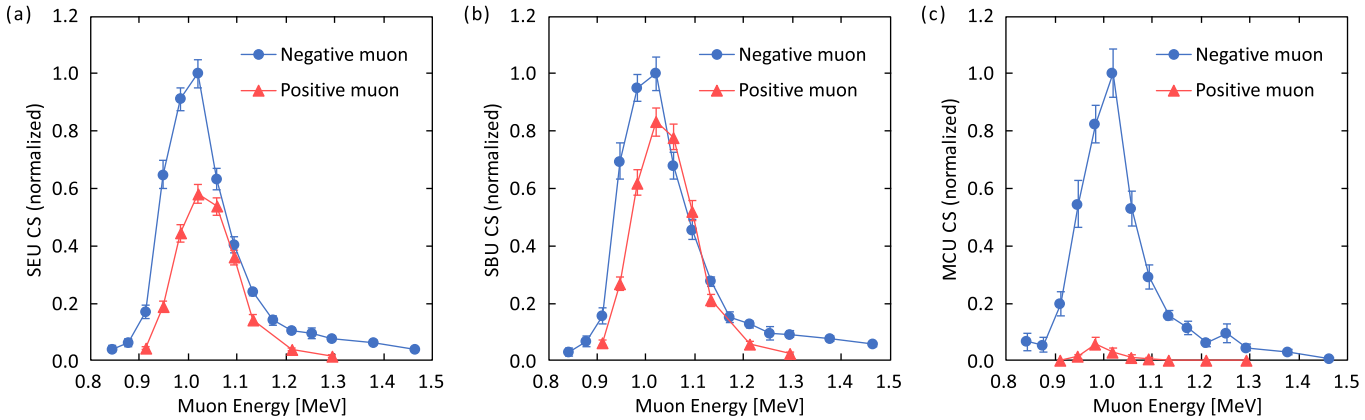

Fig. 4. (a) SEU, (b) SBU, (c) MCU CSs as a function of muon energy. Blue and red symbols are for negative and positive muons, respectively. Each CS is normalized by the CS value at 1.02 MeV of the negative muon. Supply voltage and data pattern are 0.35 V and All0, respectively. Error bars represent one standard error.

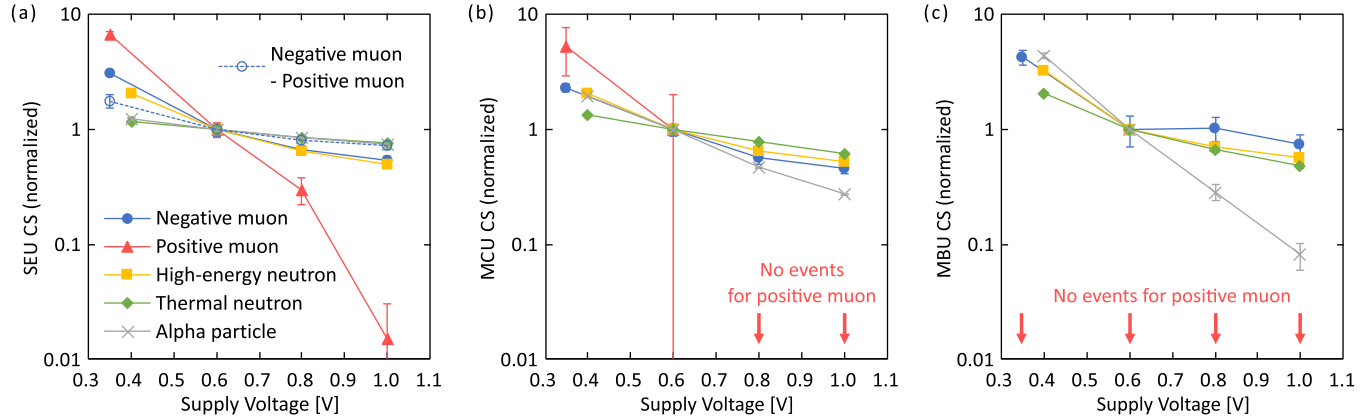

Fig. 5. (a) SEU, (b) MCU, and (c) MBU CSs as a function of supply voltage. Blue and red symbols are for negative and positive muons, respectively. Yellow and green symbols are for high-energy and thermal neutrons, respectively. Gray symbols are for alpha particles. Open circles are for the difference between the negative and positive muons: CS(negative muon) − CS(positive muon). The CSs are normalized in each particle by the respective CS value at 0.6 V. The muon energy is 1.02 MeV. The data pattern is All0. Error bars represent one standard error. Note that the CS for the high-energy neutron is mostly from [22].

dependence. Fig. 5(a)–(c) present the voltage dependence of the SEU, MCU, and MBU CSs, respectively. Each graph includes the CSs for the particles listed in Table I. The data pattern was the All0 pattern. To emphasize the similarities and differences, the CSs were normalized in each particle by the respective CS value at 0.6 V.

For all the particles, the SEU CS exhibited an exponential decrease with the voltage, as seen in Fig. 5(a). Such exponential dependence has been represented in the empirical model

$$\text{SEU CS} \propto \exp(-Q_{\text{crit}}/Q_{\text{coll}}) \tag{1}$$

where Q_{crit} and Q_{coll} denote critical charge and collected charge, respectively [26]. With a first-order approximation, the critical charge can be expressed as the product of the supply voltage and the capacitance of internal nodes: $Q_{\text{crit}} \sim V_{\text{DD}} \times C_{\text{node}}$. Hence, the difference in the charge collection among the incident particles can be evaluated by comparing the slope of the voltage dependence: the steeper the slope, the smaller the collected charge. Note that, since this empirical model is a simplified equation, subtle differences in designing and manufacturing conditions can disturb the comparative evaluation of the particle-specific charge collection based on the slope. In this work, all the irradiation tests were performed using the SRAM chips with identical design from the same manufacturing lot. In this case, the difference in the slope is supposed to reflect the difference in the particle-specific charge collection, which increases with the amount of charge deposition and its collection efficiency.

The SEU CS for the positive muon drastically decreased with the voltage, which was significantly different from the other particles, as observed in Fig. 5(a). The charge deposition by the positive muon is solely due to the direct ionization, in which the LET is low. This obviously results in the small collected charge compared to the other particles. From (1), this leads to a steeper slope for the positive muon than for the other particles, which is consistent with the observed result.

In the case of the negative muon, the voltage dependence of the SEU CS was very similar to that for the high-energy neutron, as confirmed in Fig. 5(a). The muon energy in this investigation was the CS-peak energy at which the contribution of the muon capture reactions is significant, as discussed in the previous section. In this case, the variety of the produced secondary ions and their LETs probably results in the broad distribution of the charge deposition and of the resulting collection, which is completely different from the positive muon case. From (1), the similarity in the slope can be interpreted as a similar charge collection. Therefore, it is indicated that the distribution of the charge collection caused by the

negative muon is similar to that caused by the high-energy neutron.

It is worth mentioning here that the similarity in the voltage dependence of the CSs between the negative muon and the high-energy neutron was reported in [18], where the experiments were performed mostly using a monoenergetic neutron source. Our experiments, on the other hand, demonstrated the similarity using the spallation neutron source with the atmospheric-like energy spectrum.

In contrast to this similarity, the voltage dependence of the SEU CS for the negative muon was different from that for the thermal neutron and the alpha particle. This would be explained by the difference in the charge collection. Here, the similarity between the thermal neutron and the alpha particle is reasonable because the LET of the alpha particle is comparable to that of the secondary ions produced by the thermal neutron, where an alpha particle and a Li ion are produced through a neutron capture reaction of ^{10}B atoms. The key observation was that the slope for the negative muon was steeper than that for the thermal neutron and the alpha particle. Since the steeper slope corresponds to the smaller collected charge as indicated by (1), this result suggests that, in the case of the negative muon, the observed SEU events include the events induced by the smaller charge collection than the alpha particle.

To understand the steeper slope for the negative muon than for the thermal neutron and the alpha particle, the CS difference between the negative and positive muons was analyzed. In Fig. 5(a), the voltage dependence of the CS difference between the muons is shown with open circles, where the CS for the positive muon was subtracted from that for the negative muon. Since the LET of direct ionization is almost identical between the negative and positive muons, the CS difference between the muons can be considered as the contribution of the capture reactions for the negative muon. As confirmed in Fig. 5(a), the voltage dependence for this CS difference was similar to that for the thermal neutron and the alpha particle. This clearly demonstrates that the muon direct ionization differentiated the voltage dependence of the SEU CS for the negative muon from that for the thermal neutron and the alpha particle, which is consistent with the above suggestion.

It is also interesting that the slope for the high-energy neutron was steeper than that for the CS difference between the negative and positive muons. The key observations here are that the slope for the CS difference between the muons was similar to that for the alpha particle and that the slope for the high-energy neutron was steeper than that for the alpha particle. It can be deduced from these observations and (1) that the steeper slope for the high-energy neutron than for the CS difference between the muons is caused by lower-LET ions than the alpha particle, i.e. protons which lead to events with small charge collection. This is consistent with spallation reactions induced by the high-energy neutron, where the proton is the most abundant secondary ion. This result therefore indicates that the voltage dependence of the SEU CS induced by the muon capture reactions is different from that induced by the high-energy neutron due to this proton contribution. In other words, the observed similarity in the voltage dependence between the negative muon and the high-energy neutron possibly stems from the compensation between the proton contribution for the high-energy neutron and the direct ionization contribution for the negative muon. This view seems reasonable because the LET of the muon is similar to that of the proton [27].

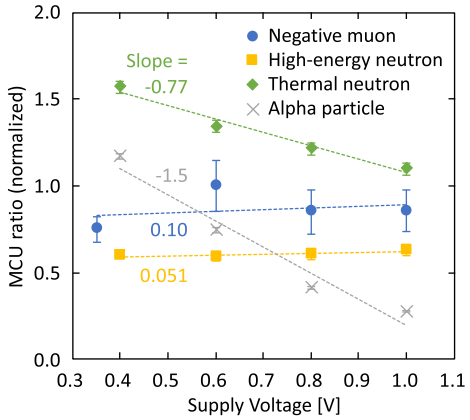

Fig. 6. MCU ratio as a function of supply voltage. Symbols are the same as Fig. 5. The values are normalized by the value at 0.6 V of the negative muon. The data pattern is All0. Error bars represent one standard error. Broken lines correspond to linear fitted curves, where the values of the slopes are noted.

Regarding the MCU and MBU CSs shown in Fig. 5(b) and (c), their voltage dependence was apparently different from the SEU CS and also between the MCU and MBU CSs. For example, the slope for the alpha particle was steeper than that for the negative muon, in contrast to the case of the SEU CS. These results indicate that the difference in the MCU and MBU responses among the particles cannot be explained simply by the difference in the charge collection evaluated based with (1). This is obvious because this empirical model cannot capture the differences in the range and emission direction of secondary ions and the resulting spatial distribution of charge collection, which are key factors determining the MCU and MBU responses. Moreover, since the MBU events are the MCU events with a specific fail bit patterns, the observed difference between the MCU and MBU responses implies the difference in the effects of these factors among the particles. This point is discussed in the following sections.

C. Analysis of MCU Ratio

MCU ratios, which were calculated by dividing the MCU CS with the SEU CS, were compared among the incident particles to investigate the difference in the MCU mechanism. The voltage dependence is compared in Fig. 6, where the data pattern was the All0 pattern. The data pattern dependence is then examined in Fig. 7. Note that the result for the positive muon is omitted because its MCU CS was significantly low.

The MCU ratio for the negative muon was larger than that for the high-energy neutron over the entire voltage range, as seen in Fig. 6. This probably reflects the difference in the emission direction of secondary ions between the muon capture reactions and the neutron spallation reactions. In the case

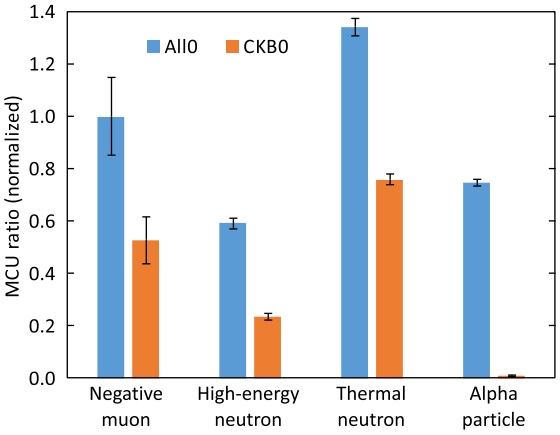

Fig. 7. Data pattern dependence of MCU ratio at 0.6 V. Cyan and orange bars are for All0 and CKB0 patterns, respectively. The values are normalized by the value of negative muon for the All0 pattern. Error bars represent one standard error.

of the muon capture reactions, the secondary ions are emitted isotropically [28].[1] In contrast, in the case of the neutron spallation reactions, the secondary ions tend to be emitted in the forward direction [29]. Since the high-energy neutron irradiation was conducted at normal incidence, the tracks of the secondary ions in the plane of the SRAM array should be shorter for the high-energy neutron than for the negative muon, which results in less chance to cause MCU events for the high-energy neutron. This leads to a higher MCU ratio for the negative muon than for the high-energy neutron, which agrees with the observed difference.

At the same time, the MCU ratio for the negative muon was lower than that for the thermal neutron over the entire voltage range. In the case of the neutron capture reaction in ^{10}B atoms, the secondary ions are emitted isotropically, as in the case of the muon capture reactions. One important point here is the location of the ^{10}B atoms. It was reported that, in advanced technologies, the ^{10}B atoms are introduced during the manufacturing process of W plugs, and hence the ^{10}B atoms are localized on the transistors within the depth range of a few hundred nanometers [13], [14], [30]. Another important point is the position of the muon stopping because the muon capture reactions can occur when the negative muon stops. Due to the energy spread of the muon beam, which includes the effect of scattering by the metal layer, the depth range of the stopping position was estimated to be larger than that of the ^{10}B atom position. It is geometrically obvious that the isotropic emissions occurred near the plane of the SRAM array are more likely to invoke the ion tracks covering the multiple SRAM cells. Therefore, the localized distribution of the ^{10}B atoms results in the higher MCU ratio for the thermal neutron compared to the negative muon, as observed in Fig. 6.

Another important finding in the voltage dependence of the MCU ratio was the difference in the slopes, the values of which are noted in Fig. 6. The slope for the negative muon was similar to that for the high-energy neutron and was $\sim$0. On the other hand, the slopes for the thermal neutron and the alpha particle were large negative values. The possible reason for this difference is the different contribution of the PBE. It is known that the PBE increases the MCU ratio and becomes more effective with increasing the voltage [31]. Hence, in terms of the slope of this voltage dependence, the negative slope can be interpreted as the small contribution of the PBE. From our results, it is speculated that the PBE contribution for the thermal neutron and the alpha particle is less significant than that for the negative muon and the high-energy neutron. This is consistent with the PBE mechanism, where relatively large charge deposition is required for well-potential perturbation. Since the muon capture reactions produce the secondary ions with higher-LET than alpha particles and Li ions, the PBE contribution can be larger for the negative muon than for the thermal neutron and the alpha particle. At the same time, the similarity in the slope between the negative muon and the high-energy neutron indicates that the PBE contribution is comparable between them.

The data pattern dependence of the MCU ratio also showed interesting differences among the incident particles. Fig. 7 presents the MCU ratios for the All0 and CKB0 patterns at 0.6 V. For all the particles, the MCU ratio for the All0 pattern was higher than that for the CKB0 pattern. This reflects the difference in the arrangement of node voltages between the data patterns [see Fig. 2]. Since SEU occurrence in SRAM cells is basically dominated by charge collection in nMOS transistors of high nodes, a smaller distance between neighboring high nodes results in a higher probability in MCU occurrence. In this case, the distance between the neighboring high nodes is smaller for the All0 pattern than for the CKB0 pattern, leading to the higher MCU ratio for the All0 pattern.

The key observation in this data pattern dependence was the difference in the relative magnitude between the MCU ratios for the All0 and CKB0 patterns. In the case of the negative muon, the MCU ratio for the CKB0 pattern was approximately half that for the All0 pattern, which was almost the same as the case of the thermal neutron. In the case of the high-energy neutron, the ratio for the CKB0 pattern was less than half that for the All0 pattern. In the case of the alpha particle, the ratio for the CKB0 pattern was significantly low. From the comparison between the thermal neutron and the alpha particle, it can be deduced that, for the thermal neutron, the relatively high MCU ratio for the CKB0 pattern is due to the isotropic emission of the secondary ions because the LET of the alpha particle is comparable to that of the secondary ions produced by the thermal neutron. Therefore, the similarity between the negative muon and the thermal neutron possibly indicates the impact of the isotropic ion emission of the muon capture reactions on the MCU response.

D. Analysis of MCU Characteristics

In the previous section, it is indicated that the contributing factors for the negative muon-induced MCUs are the PBE and the isotropic emission of the secondary ions. To explore these

[1]When a negative muon is injected into matter and loses its kinetic energy, the muon is captured by the Coulomb field of the nucleus, forming a muonic atom. After the muon reaches the 1*s* state of the muonic atom, it is most likely captured by a bound proton. This reaction excites the nucleus and results in the production of secondary particles which are emitted isotropically.

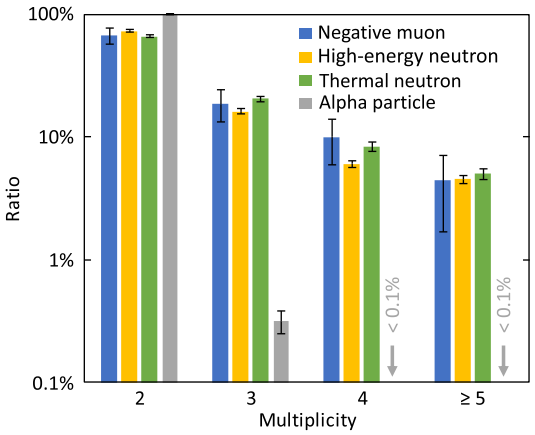

Fig. 8. Multiplicity distribution of MCU events. Blue bars are for negative muons. Yellow and green bars are for high-energy and thermal neutrons, respectively. Gray bars are for alpha particles. All ratios are the values averaged in the voltage range ≥0.6 V. 100% corresponds to the total MCU events. The data pattern is All0. Error bars represent one standard error.

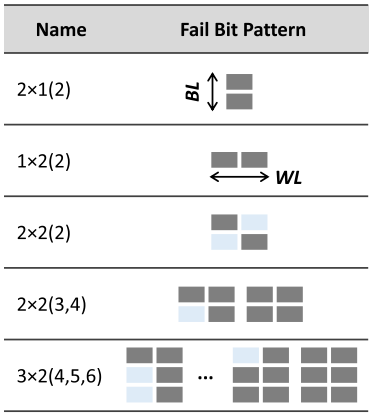

Fig. 9. Groups of fail bit patterns. Rectangular cells are SRAM cells. Gray cells represent fail bits. Vertical and horizontal directions are parallel to BL and WL directions, respectively. The mirror images of each pattern are included in the same group.

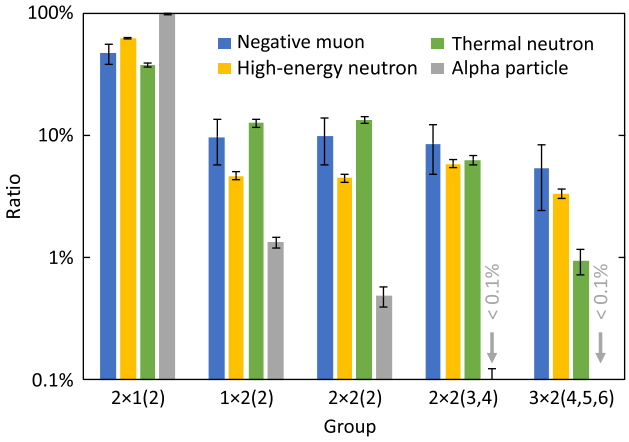

Fig. 10. Ratios for MCU groups shown in Fig. 9. The color for each particle is the same as used in Fig. 8. All ratios are the values averaged in the voltage range ≥0.6 V. 100% corresponds to the total MCU events. The data pattern is All0. Error bars represent one standard error.

factors in more detail, the MCU events were analyzed in terms of the multiplicity and the fail bit pattern. This analysis was conducted for the All0 pattern.

In the multiplicity distribution shown in Fig. 8, the negative muon exhibited a similar trend with the high-energy neutron and the thermal neutron, where the MCU events with high multiplicities were found. In the case of the alpha particle, almost all the MCU events were with the multiplicity of 2. This result clearly demonstrates that the high-multiplicity events for the negative muon were induced by the secondary ions produced through the muon capture reactions.

When focusing on the difference between the high-energy neutron and the thermal neutron, the ratios at the multiplicities of 3 and 4 were higher for the thermal neutron, whereas the ratio at the multiplicity of ≥5 is similar between them. This can be explained by the larger contribution of the PBE for the high-energy neutron because the PBE increases the multiplicity of MCU events [9]. For the negative muon, the PBE contribution is indicated to be comparable to that for the high-energy neutron in the previous section. On the other hand, no distinguishable difference was observed in the multiplicity distribution between the negative muon and the thermal neutron. To elucidate this point, the fail bit patterns were compared.

The fail bit patterns of the MCU events were analyzed according to the classification shown in Fig. 9, where the five groups were named as "BL-range × WL-range(multiplicity)." The ratios of these MCU groups for the incident particles are presented in Fig. 10.

The ratio of the 2 × 1(2) group was the highest for all the particles. This is obvious from the physical range of the pattern. As illustrated in Fig. 9, due to the rectangular shape of the SRAM cells, the physical range of the 2 × 1(2) group is the shortest among the five groups. In the case of the alpha particle, the ratio of this 2 × 1(2) group was approximately 98%. As discussed in Fig. 7, the difference between the thermal neutron and the alpha particle can be considered as the impact of the isotropic ion emission. Therefore, for the thermal neutron, the relatively high ratios in the other four groups are very likely due to the isotropic ion emission.

In the 1 × 2(2) and 2 × 2(2) groups, the ratio for the negative muon was similar to that for the thermal neutron, rather than that for the high-energy neutron. This indicates that, for the negative muon, these MCU groups were mainly due to the isotropic emission of the secondary ions. Similarly, the impact of the isotropic emission was suggested in the data pattern dependence of the MCU ratio in Fig. 7, where the MCU ratio for the CKB0 pattern was relatively high. This is consistent with this pattern analysis because the 2×2(2) group corresponds to the pattern of neighboring high nodes in the CKB0 pattern [see Fig. 2(b)].

In the 2×2(3,4) and 3×2(4,5,6) groups, on the other hand, the ratio for the negative muon was comparable to that for the high-energy neutron. In particular, in the 3 × 2(4,5,6) group, the ratio for the thermal neutron was apparently lower than that for the negative muon and the high-energy neutron. The common feature of the 2 × 2(3,4) and 3 × 2(4,5,6) groups is the non-linear shape of the fail bit patterns, which cannot be explained by linear ion tracks. The key point here is

that this type of patterns increases with increasing the PBE contribution because the PBE is activated by well-potential perturbation and multiple nodes in the same well can be simultaneously affected by the PBE [32]. The observed ratios of these groups therefore indicate that the PBE contribution is higher for the negative muon and the high-energy neutron than for the thermal neutron. This agrees with the discussion in the previous section, where the higher PBE contribution for the negative muon and the high-energy neutron was indicated in the voltage dependence of the MCU ratio in Fig. 6.

From our results, it is probable that, for the negative muon, the MCU characteristics are dominated by the nature of the muon capture reactions, where both the isotropic ion emission and the PBE triggered by high-LET ions are important factors. The high-energy neutron does not possess the isotropic emission of the secondary ions. The thermal neutron does not produce the secondary ions with LET enough for triggering the PBE. For these reasons, the MCU response to the negative muon is different from that to the high-energy neutron and the thermal neutron, as observed in this study.

IV. Conclusion

We have experimentally investigated the muon-induced SEUs in the 20-nm bulk planar SRAMs. The SEU, MCU, and MBU CSs for the negative and positive muons have been compared with those for the high-energy neutron, the thermal neutron, and the alpha particle. The MCU events have been characterized in terms of the multiplicity and the fail bit pattern. The mechanisms of the muon-induced SEUs and MCUs have been explored through the comparison of the SEU and MCU responses among the incident particles.

The muon energy dependence of the CSs has clearly confirmed the Bragg peak effect for both the negative and positive muons and the significant contribution of the muon capture reactions to the MCU CS for the negative muon, as similarly reported in the previous studies. We have found that the positive muon induces the MCU events in the 20-nm planar SRAMs, whereas no MCU events were observed in the previous studies of the 65- and 28-nm planar SRAMs. This difference has been attributed to the scaling of the SRAM cells, which suggests that the positive muon-induced MCUs may increase in more advanced technologies. On the basis of the empirical relation between the SEU CS and the charge collection, the similarities and differences in the voltage dependence of the SEU CS among the particles have been explained by the contributing secondary ions and their LETs. The detailed analyses of the MCU ratio and the fail bit patterns have revealed that both the PBE and the isotropic emission of the secondary ions have an important role for the characteristics of the negative muon-induced MCUs.

In conclusion, we have demonstrated that the SEU and MCU responses to the negative and positive muons are essentially different from that to the other terrestrial radiations: the high-energy neutron, the thermal neutron, and the alpha particle. In particular, we have determined that the unique nature of the muon capture reactions, i.e. the high-LET ion production and the isotropic ion emission, differentiates the MCU characteristics for the negative muon from that for the high-energy neutron and the thermal neutron.

Acknowledgment

The muon experiment at the Materials and Life Science Experimental Facility of the J-PARC was performed under the S1 type research project, KEK (Proposal No. 2014MS01). The authors would like to thank Dr. W. Liao of Kochi University of Technology for the advice on the muon irradiation test. They would like to thank Dr. I. Umegaki of Toyota Central R&D Labs., Inc. and S. Doiuchi of Muon Science Laboratory for the assistance at MUSE. They would also like to thank Prof. M. Fukuda of Osaka University for the support at RCNP.

References

[1] J. F. Ziegler, "Terrestrial cosmic rays," *IBM J. Res. Develop.*, vol. 40, no. 1, pp. 19–40, Jan. 1996.

[2] G. Hubert, L. Artola, and D. Regis, "Impact of scaling on the soft error sensitivity of bulk FDSOI and FinFET technologies due to atmospheric radiation," *Integr. VLSI J.*, vol. 50, pp. 39–47, Jun. 2015.

[3] A. Infantino, R. G. Alia, and M. Brugger, "Monte Carlo evaluation of single event effects in a deep-submicron bulk technology: Comparison between atmospheric and accelerator environment," *IEEE Trans. Nucl. Sci.*, vol. 64, no. 1, pp. 596–604, Jan. 2017.

[4] W. Liao *et al.*, "Measurement and mechanism investigation of negative and positive muon-induced upsets in 65-nm bulk SRAMs," *IEEE Trans. Nucl. Sci.*, vol. 65, no. 8, pp. 1734–1741, Aug. 2018.

[5] S. Manabe *et al.*, "Negative and positive muon-induced single event upsets in 65-nm UTBB SOI SRAMs," *IEEE Trans. Nucl. Sci.*, vol. 65, no. 8, pp. 1742–1749, Aug. 2018.

[6] W. Liao *et al.*, "Negative and positive muon-induced SEU cross sections in 28-nm and 65-nm planar bulk CMOS SRAMs," in *Proc. IEEE Int. Rel. Phys. Symp. (IRPS)*, Mar. 2019, p. 5A.

[7] T. Mahara *et al.*, "Irradiation test of 65-nm bulk SRAMs with DC muon beam at RCNP-MuSIC facility," *IEEE Trans. Nucl. Sci.*, vol. 67, no. 7, pp. 1555–1559, Jul. 2020.

[8] K. Osada, K. Yamaguchi, Y. Saitoh, and T. Kawahara, "SRAM immunity to cosmic-ray-induced multierrors based on analysis of an induced parasitic bipolar effect," *IEEE J. Solid-State Circuits*, vol. 39, no. 5, pp. 827–833, May 2004.

[9] G. Gasiot, D. Giot, and P. Roche, "Multiple cell upsets as the key contribution to the total SER of 65 nm CMOS SRAMs and its dependence on well engineering," *IEEE Trans. Nucl. Sci.*, vol. 54, no. 6, pp. 2468–2473, Dec. 2007.

[10] *Measurement and Reporting of Alpha Particle and Terrestrial Cosmic Ray-Induced Soft Errors in Semiconductor Devices*, JEDEC Standard JESD89A, Oct. 2006.

[11] R. C. Baumann and E. B. Smith, "Neutron-induced boron fission as a major source of soft errors in deep submicron SRAM devices," in *Proc. IEEE Int. Rel. Phys. Symp. 38th Annu.*, Apr. 2000, pp. 152–157.

[12] S.-J. Wen, R. Wong, M. Romain, and N. Tam, "Thermal neutron soft error rate for SRAMs in the 90nm–45nm technology range," in *Proc. IEEE Int. Rel. Phys. Symp.*, May 2010, p. SE.

[13] S.-J. Wen, S. Y. Pai, R. Wong, M. Romain, and N. Tam, "B10 finding and correlation to thermal neutron soft error rate sensitivity for SRAMs in the sub-micron technology," in *Proc. IEEE Int. Integr. Rel. Workshop Final Rep.*, Oct. 2010, pp. 31–33.

[14] Y.-P. Fang and A. S. Oates, "Thermal neutron-induced soft errors in advanced memory and logic devices," *IEEE Trans. Device Mater. Rel.*, vol. 14, no. 1, pp. 583–586, Mar. 2014.

[15] N. Seifert, S. Jahinuzzaman, J. Velamala, and N. Patel, "Susceptibility of planar and 3D tri-gate technologies to muon-induced single event upsets," in *Proc. IEEE Int. Rel. Phys. Symp.*, Apr. 2015, p. 2C.

[16] G. Gasiot, D. Soussan, J.-L. Autran, V. Malherbe, and P. Roche, "Muons and thermal neutrons SEU characterization of 28nm UTBB FD-SOI and bulk eSRAMs," in *Proc. IEEE Int. Rel. Phys. Symp.*, Apr. 2015, p. 2C.

[17] S. Manabe, Y. Watanabe, W. Liao, M. Hashimoto, and S.-I. Abe, "Estimation of muon-induced SEU rates for 65-nm bulk and UTBB-SOI SRAMs," *IEEE Trans. Nucl. Sci.*, vol. 66, no. 7, pp. 1398–1403, Jul. 2019.

[18] W. Liao, M. Hashimoto, S. Manabe, S.-I. Abe, and Y. Watanabe, "Similarity analysis on Neutron- and negative muon-induced MCUs in 65-nm bulk SRAM," *IEEE Trans. Nucl. Sci.*, vol. 66, no. 7, pp. 1390–1397, Jul. 2019.

[19] Y. Miyake *et al.*, "J-PARC muon facility, MUSE," *Phys. Procedia*, vol. 30, pp. 46–49, Jun. 2012.

[20] M. Tampo *et al.*, "The development of a non-destructive analysis system with negative muon beam for industrial devices at J-PARC MUSE," in *Proc. 2nd Int. Symp. Sci.*, vol. 8, Sep. 2015, Art. no. 036016.

[21] Y. Iwamoto *et al.*, "Evaluation of the white neutron beam spectrum for single-event effects testing at the RCNP cyclotron facility," *Nucl. Technol.*, vol. 173, no. 2, pp. 210–217, Feb. 2011.

[22] T. Kato, T. Yamazaki, N. Saito, and H. Matsuyama, "Neutron-induced multiple-cell upsets in 20-nm bulk SRAM: Angular sensitivity and impact of multiwell potential perturbation," *IEEE Trans. Nucl. Sci.*, vol. 66, no. 7, pp. 1381–1389, Jul. 2019.

[23] Y. Sakurai and T. Kobayashi, "Characteristics of the KUR heavy water neutron irradiation facility as a neutron irradiation field with variable energy spectra," *Nucl. Instrum. Methods Phys. Res. A, Accel. Spectrom. Detect. Assoc. Equip.*, vol. 453, no. 3, pp. 569–596, Oct. 2000.

[24] T. Sato, "Analytical model for estimating terrestrial cosmic ray fluxes nearly anytime and anywhere in the world: Extension of PARMA/EXPACS," *PLoS ONE*, vol. 10, no. 12, Dec. 2015, Art. no. e0144679.

[25] O. A. Amusan *et al.*, "Charge collection and charge sharing in a 130 nm CMOS technology," *IEEE Trans. Nucl. Sci.*, vol. 53, no. 6, pp. 3253–3258, Dec. 2006.

[26] P. Hazucha and C. Svensson, "Impact of CMOS technology scaling on the atmospheric neutron soft error rate," *IEEE Trans. Nucl. Sci.*, vol. 47, no. 6, pp. 2586–2594, Dec. 2000.

[27] B. D. Sierawski *et al.*, "Muon-induced single event upsets in deep-submicron technology," *IEEE Trans. Nucl. Sci.*, vol. 57, no. 6, pp. 3273–3278, Dec. 2010.

[28] D. Measday, "The nuclear physics of muon capture," *Phys. Rep.*, vol. 354, nos. 4–5, pp. 243–409, Nov. 2001.

[29] Y. Watanabe *et al.*, "Light ion production in 175 MeV quasi mono-energetic neutron induced reactions on carbon, oxygen, and silicon," *Prog. Nucl. Sci. Technol.*, vol. 47, no. 6, pp. 2586–2594, Dec. 2000.

[30] T. Yamazaki *et al.*, "Origin analysis of thermal neutron soft error rate at nanometer scale," *J. Vac. Sci. Technol. B, Microelectron.*, vol. 33, no. 2, Mar. 2015, Art. no. 020604.

[31] T. Nakauchi, N. Mikami, A. Oyama, H. Kobayashi, H. Usui, and J. Kase, "A novel technique for mitigating neutron-induced multi-cell upset by means of back bias," in *Proc. IEEE Int. Rel. Phys. Symp.*, Apr./May 2008, pp. 187–191.

[32] T. Kato, M. Hashimoto, and H. Matsuyama, "Angular sensitivity of neutron-induced single-event upsets in 12-nm FinFET SRAMs with comparison to 20-nm planar SRAMs," *IEEE Trans. Nucl. Sci.*, vol. 67, no. 7, pp. 1485–1493, Jul. 2020.